Published by JScE as Proceedings of 4th International Conference on Earthquake Engineering and Post-Disaster Reconstruction Planning (ICEE-PDRP), 19-21 Jan. 2026, Bhaktapur, Nepal

SEISMIC MICROZONATION OF KATHMANDU VALLEY: INTEGRATION OF BOREHOLE DATA, MICROTREMOR SURVEY, AND NUMERICAL EVALUATION

Sanjeeb Pudasaini[1]*, Khem Raj Pokharel[1], Ram Chandra Tiwari[1], Aanchal Tiwari[1], Sandeep Sapkota[2]

[1] Department of Civil Engineering, Institute of Engineering, Pulchowk Campus, Tribhuvan University, Nepal
[2] Department of Civil Engineering, Universal College of Science & Technology, Pokhara University, Nepal

Abstract

This Kathmandu Valley by integrating borehole data, microtremor survey results, and numerical evaluation techniques to assess soil liquefaction potential. Microtremor measurements were collected from 75 stations throughout the valley, and the vulnerability index (K_g) was calculated using Nakamura's method, which factors in fundamental frequency and amplification characteristics. The resulting values ranged from 0.091 to 13.463, highlighting the varying liquefaction risk across the valley. Borehole data from 29 excavation sites were used to validate the liquefaction potential, and a threshold value was established in alignment with prior research benchmarks. Numerical evaluation through finite element modeling (FEM) using PLAXIS-2D was performed to further assess liquefaction susceptibility. The FEM analysis confirmed areas with a value greater than 5 as highly vulnerable to liquefaction, while other regions exhibited low susceptibility. Liquefaction susceptibility maps identified critical high-risk zones, particularly in Kathmandu, including areas near Kantipath, Maitighar, and Teku, as well as in Lalitpur and Bhaktapur, such as near Chakupat, Patan Durbar Square, and Bhaktapur Durbar Square. This study demonstrates that integrating microtremor survey data, borehole information, and numerical analysis offers a comprehensive, reliable approach for seismic microzonation and liquefaction risk assessment in earthquake-prone regions like Kathmandu Valley.

Keywords: Seismic microzonation; Liquefaction potential; Microtremor (HVSR) survey; Finite Element Modeling (FEM); Kathmandu Valley sediments

1. Introduction

Kathmandu Valley, situated in a seismically active region of Nepal, is particularly vulnerable to soil liquefaction due to its soft lacustrine and fluvial sediments. The valley's susceptibility to liquefaction has been highlighted in several studies, including those by Piya et al. (2004) and Subedi and Acharya (2022), who emphasized the need for comprehensive hazard assessments. Liquefaction, a phenomenon where saturated soils lose strength during seismic events, poses significant risks to infrastructure and heritage sites in the valley. The 2015 Gorkha earthquake underscored these risks, with documented liquefaction occurrences in areas such as Manamaiju and Imadol, as reported by Gautam et al. (2017) and Sharma et al. (2016). These events highlighted the importance of accurate liquefaction susceptibility mapping to inform disaster preparedness and urban planning.

Traditional liquefaction hazard assessments often rely on borehole data and geotechnical investigations, which can be time-consuming and costly. In response, geophysical methods, particularly microtremor surveys, have emerged as efficient tools for rapid and cost-effective evaluation of subsurface conditions. Microtremor measurements, as discussed by Nakamura (1989) and Beroya et al. (2009), offer a non-invasive means to estimate soil properties related to seismic response.

This study aims to integrate microtremor data with numerical modeling to assess liquefaction potential

*Corresponding author: Sanjeeb Pudasaini
Affiliation: IOE, Pulchowk Campus, Tribhuvan University
Email: 078msgt3012.sanjeeb@gmail.com
https://doi.org/10.3126/jsce.v13i1.89628

Figure 1. Study area-map of Nepal highlighting Kathmandu valley

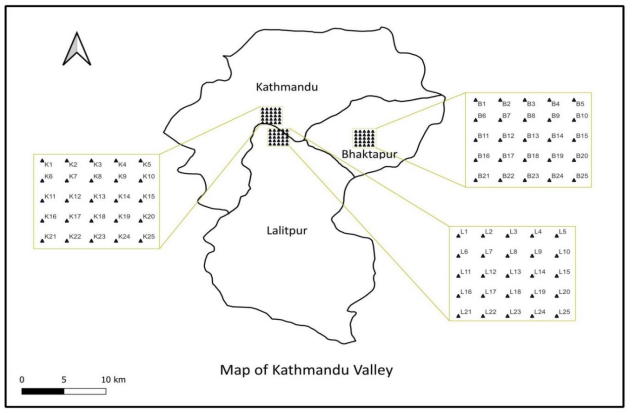

Figure 2. Survey location within the Kathmandu valley

in the core areas of Kathmandu Valley, focusing on Kathmandu, Bhaktapur, and Lalitpur districts. By employing microtremor surveys and finite element analysis using PLAXIS-2D, the research seeks to provide a comprehensive liquefaction hazard map. The findings will contribute to the validation of microtremor-based assessments and support informed decision-making for mitigating liquefaction risks in the valley.

2. Study Area

The study area encompasses the core regions of Kathmandu, Bhaktapur, and Lalitpur districts, specifically including the areas around their respective Durbar Squares. Each district is divided into a 5x5 grid, with grid points spaced 500 meters apart. For each area, 25 microtremor stations were established, numbered 1 to 25, and labeled with the codes K, B, and L to represent Kathmandu, Bhaktapur, and Lalitpur, respectively (Figure 1 & 2).

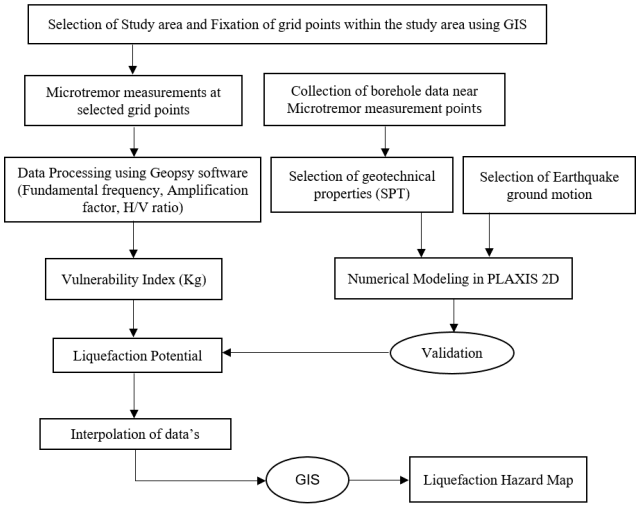

Figure 3. Flow chart of methodology

3. Methodology

The methodology of this study is summarized in the flow diagram on the next page (Figure 3). It begins with a comprehensive literature review to identify existing research gaps and define clear objectives. This is followed by data collection, including microtremor measurements, borehole information, and earthquake records. Finally, numerical modeling and dynamic analysis are conducted using PLAXIS-2D, incorporating empirical correlations and validated soil parameters to assess liquefaction susceptibility.

In this study, clay and silt layers were modeled using the Generalized Hardening Soil model, while sand layers were simulated with the UBC3D-PLM model (Table 1) to analyze liquefaction potential. The selection of constitutive models was guided by soil type and the demands of dynamic analysis in PLAXIS-2D. The UBCSAND 904aR model, used for sand, effectively captures cyclic strain accumulation and excess pore pressure generation under undrained conditions, with parameters calibrated based on normalized SPT values $(N1)_{60}$.

The Generalized Hardening Soil (GHS) model is a flexible, user-defined extension of the HSsmall model, allowing customized stress-strain configurations and yield functions (Table 2). Its parameters are partly derived from empirical correlations.

A Linear Elastic model is used to represent the underlying rock layer at the base of the domain, simulating high shear wave velocity conditions typically greater than 800 m/s (Table 3). A 1-meter thick bedrock layer is included

Table 1. Soil parameters and equations

Soil Parameters	Equations
Peak Friction Angle (ϕ)	$\phi = 27.1 + 0.3N_{60} - 0.0054N_{60}^2$
Constant Volume Friction Angle (ϕ_{cv})	$\phi_{cv} = \phi - (10° + \max(0, (N_{60} - 15)))$
Elastic Shear Modulus (G^e)	$G^e = 2.17 \times 20 \times (N_{60})^{0.333}$
Elastic Bulk Modulus (K^e)	$K^e = 0.7G^e$
Plastic Shear Modulus (G^p)	$G^p = G^e \times (N_1)^2 \times 0.003 + 100$
Failure Ratio (R_f)	$R_f = 1.1 \times (N_{60})^{0.15}$
Power for stress dependency (m)	0.5
Power for stress dependency (n)	0.4
Densification factor (f_{acbd})	1.0
Densification factor (f_{acpost})	1.0
Densification factor (f_{acpf})	1.0

Table 2. Soil parameters, equations, and units

Soil Parameters	Equations	Units
Tangent stiffness for standard drained triaxial (E_{50}^{ref})	900(N, M.Z.2012)	kNm
Unloading reloading stiffness (E_{ur})	$3E_{50}^{\text{ref}}$	kNm
Power for stress-level dependency of stiffness (m)	0.6	–
Cohesion (c)	0	kPa
Friction angle (ϕ)	30	°
Dilatancy angle (ψ)	0	°
Shear strain in which $G = 0.722G_0$ ($\gamma_{0.7G_0}$)	0.0007	–
Poisson's ratio (ν)	0.2	–
Reference stress (p_{ref})	100	kPa
Failure ratio (R_f)	0.9	–
Over consolidation ratio (OCR)	1	–
Pre-overburden pressure (POP)	0	–
Poisson's coefficient (K)	0.73	–
Stress dependent stiffness	1	–
Stress dependency formula	1	–
Plasticity model	1	E_u

above a compliant base boundary, which uses prescribed displacements and viscous dashpots to apply earthquake motion while minimizing wave reflections (Bentley Systems Incorporated, 2020).

Table 3. Model parameters for linear elastic model

Parameters	Name	Value	Unit
Material Model	Name	Linear Elastic	–
Type of material behavior	Type	Drained	–
Total unsaturated unit weight of soil	γ_{unsat}	22	kN/m^3
Elastic Modulus of soil	E	80000	kN/m^2
Poisson's ratio	ν	0.2	–

The input motion used is the 2015 Gorkha earthquake accelerogram (Mw 7.8, PGA 0.18g) recorded at Kantipath, Kathmandu, with an epicentral distance of 59.9 km. It is applied as half the outcrop motion at the compliant base using a prescribed displacement of 0.5 m in the x-direction, with the y-direction fixed, and modeled through a dynamic multiplier (Figure 4). In this study, a very coarse mesh was

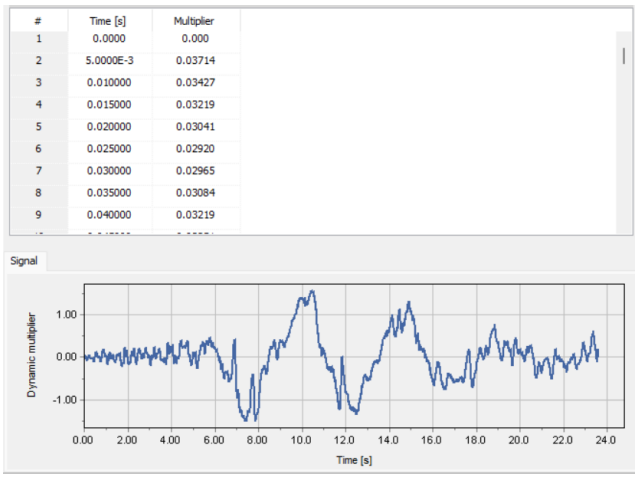

Figure 4. Input motion of Gorkha, Nepal Earthquake 2015

adopted to balance accuracy with computational efficiency, as dynamic analyses in PLAXIS-2D are significantly more time-consuming than static ones (Figure 5). While fine meshes enhance result precision, the coarse mesh was sufficient for the liquefaction analysis without excessively increasing runtime.

In this study, vertical boundaries were fixed while the base was modeled as a compliant boundary to absorb outgoing seismic waves. The dynamic phase used a prescribed displacement as input, and tied degrees of freedom were applied to simulate symmetry. PLAXIS automatically managed time stepping based on element size and material properties to ensure stable dynamic calculations.

The microtremor results were used to determine the predominant frequency (F_p) and amplification factor (A_p) at each observation site. The vulnerability index (Kg) was then calculated to assess the potential for liquefaction. The

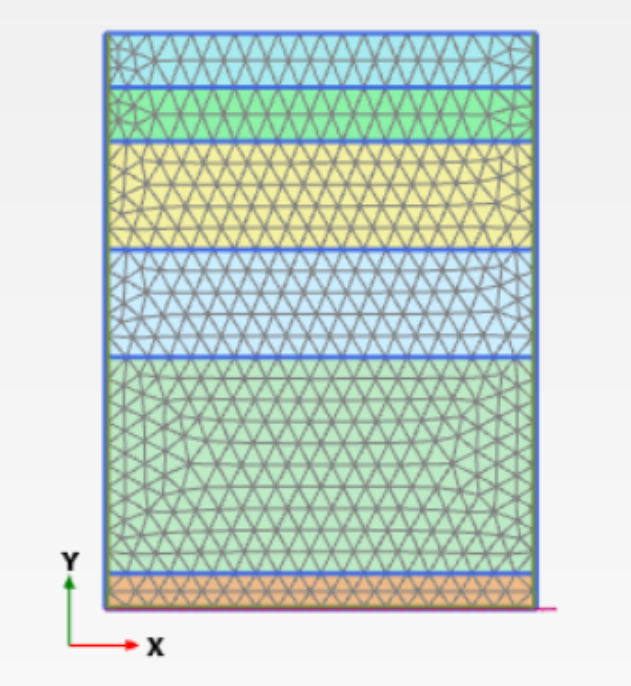

Figure 5. Generated mesh in PLAXIS-2D

Kg value serves as an indicator of liquefaction extent and earthquake-induced ground damage, where higher values signify greater vulnerability (Nakamura, 1989, Rezaei and Choobbasti, 2014). Its spatial distribution helps identify weak zones susceptible to damage (Beroya et al., 2009). The vulnerability index is defined as follows:

$$K_g = \frac{A_p^2}{F_p} \tag{1}$$

Similarly, the liquefaction potential can be expressed by means of excess pore pressure ratio r_u which represents the ratio of the excess pore pressure and the initial vertical stress at that depth (Laera and Brinkgreve, 2015). For UBC-3D PLM ru is given by,

$$r_u = 1 - \frac{\sigma'_v}{\sigma'_{vo}} \tag{2}$$

Where σ'_v is the vertical stress at the end of dynamic calculation and σ'_{vo} is the initial vertical stress prior to the seismic motion. When $r_u = 1$ the corresponding layer is in a complete liquefied state.

4. Result and Discussion

This section presents and analyzes results from microtremor measurements and PLAXIS-2D simulations. The vulnerability index (K_g) is correlated with liquefaction susceptibility, and a GIS-based map illustrates the spatial distribution of Kg and borehole liquefaction potential. A threshold Kg value for liquefaction is also determined. The vulnerability index (K_g) of the various stations are listed below in Table 4.

To analyze the correlation between the microtremor-derived vulnerability index (K_g) and liquefaction susceptibility, the K_g values were interpolated and mapped using ArcGIS. These maps were then examined to identify the range of K_g values associated with liquefaction occurrences in the three core study areas (Figure 6). Similar maps can be prepared for Bhaktapur and Lalitpur core areas.

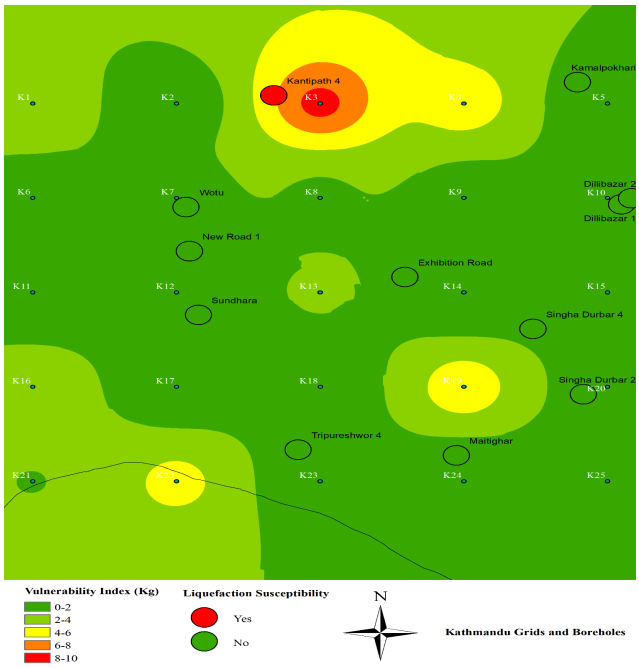

Figure 6. Vulnerability index and liquefaction susceptibility map of Kathmandu core

Following the 2015 Gorkha Earthquake, multiple sites within the valley experienced liquefaction (Table 5). The locations and details of these affected sites are listed below for validation purposes. Table 6 shows the vulnerability index of Liquefied site in Gorkha Earthquake 2015.

5. Conclusion

This study found that the vulnerability index (Kg) in the core areas of Kathmandu Valley (Table 6) ranges from 0.091 to 13.463. Finite element analysis using PLAXIS-2D indicates that several boreholes are susceptible to liquefaction, especially in areas where the vulnerability index exceeds 5. The combined analysis shows that zones with $K_g > 5$ correspond to high liquefaction susceptibility, while areas with lower Kg values are less vulnerable.

Specifically, within the Kathmandu core, pockets near Kantipath, Maitighar, and Teku (close to the Bagmati

Table 4. Vulnerability index from microtremor measurements

Location	Station	Latitude	Longitude	E_p	A_p	K_g
Bhaktapur Grids						
Bhaktapur	B3	27.681027	85.428143	0.456068	1.96998	8.509
Bhaktapur	B9	27.676530	85.433221	0.463575	1.7612	6.779
Lalitpur Grids						
Lalitpur	L3	27.6823940	85.325094	0.5111	2.3728	11.016
Lalitpur	L12	27.6734000	85.319410	0.26347	1.89363	13.463
Kathmandu Grids						
Kathmandu	K3	27.7103610	85.316090	0.66934	2.39855	8.667
Kathmandu	K4	27.7103610	85.321090	0.35449	1.33271	5.010

Table 5. List of liquefied sites in Kathmandu valley

Site	Latitude	Longitude	Epicentral distance (km)	Evidence type
Duwakot	27°42′34.0″	85°25′30.3″	56.57	Sand boils
Mulpani	27°42′16.5″	85°23′58.6″	56.92	Sand boils
Ramkot	27°42′39.7″	85°15′42.0″	75.80	Sand boils
Manamaiju	27°44′43.9″	85°18′08.0″	70.35	Sand boils / Lateral spreading
Bungamati	27°37′43.1″	85°17′49.7″	81.22	Sand boils
Imadol	27°40′00.8″	85°20′16.4″	75.4	Sand boils
Latkothban	27°39′20.4″	85°20′30.9″	76.68	Sand boils
Lakankthali	27°40′29.3″	85°21′45.5″	73.42	Lateral spreading
Guheshwori	27°42′33.3″	85°21′27.2″	59.6	Sand boils

Table 6. Vulnerability index of liquefied site in Gorkha earthquake 2015

Location	Station	Latitude	Longitude	E_p	A_p	K_g	Remarks
Lalitpur	Imadol	27.66032	85.37855	0.32255	1.3997	5.843	$K_g - 5$
Lalitpur	Hatiban	27.65513	85.33484	1.0758	2.3650	5.052	$K_g > 5$

River at the junction of Kathmandu and Lalitpur) exhibit significant liquefaction risk. In Lalitpur, areas around Chakupat, Patan Durbar Square, and between Balkumari and Imadol near the rivulet banks show high susceptibility. Similarly, in Bhaktapur, zones near Bhaktapur Durbar Square and pockets between Jagati and Suryabinayak are vulnerable.

The strong correlation between microtremor-derived Kg values and PLAXIS-2D results confirms microtremor surveys as an effective, non-invasive, and cost-efficient method for liquefaction assessment. Given rapid urbanization and critical infrastructure in the region, these findings are vital for disaster management and urban planning. Thus, wider adoption of microtremor-based assessments is recommended across Nepal's seismic-prone areas to enhance earthquake resilience.

References

Bentley Systems Incorporated (Ed.). (2020). *Plaxis 2d reference manual*. Bentley Systems Incorporated.

Beroya, M. A., Aydin, A., Tiglao, R., & Lasala, M. (2009). Use of microtremor in liquefaction hazard mapping. *Engineering Geology*, *107*(3–4), 140–153. https://doi.org/10.1016/j.enggeo.2009.04.009

Gautam, D., Chaulagain, H., & Rodrigues, H. (2017). Seismic vulnerability and post-earthquake damage assessment of kathmandu valley's historic masonry buildings. *Journal of Building Engineering*, *13*, 1–10. https://doi.org/10.1016/j.jobe.2017.06.003

Laera, A., & Brinkgreve, R. (Eds.). (2015). *Plaxis site response analysis and liquefaction evaluation 2015*. PLAXIS.

Nakamura, Y. (1989). A method for dynamic characteristics estimation of subsurface using microtremor on the ground surface [Available at https://trid.trb.org/view/294184]. *Railway Technical Research Institute Quarterly Reports*, *30*(1), 25–33.

Piya, B., van Westen, C., & Woldai, T. (2004). Geological database for liquefaction hazard analysis in the kathmandu valley, nepal. *Journal of Nepal Geological Society*, *30*, 141–152. https://doi.org/10.3126/jngs.v30i0.31704

Rezaei, S., & Choobbasti, A. J. (2014). Liquefaction assessment using microtremor measurement, conventional method and artificial neural network (case study: Babol, iran). *Frontiers of Structural and Civil Engineering*, *8*(3), 292–307. https://doi.org/10.1007/s11709-014-0256-8

Sharma, K., Deng, L., & Qin, X. (2016). Ground motion and damage pattern during the 2015 gorkha nepal earthquake. *Frontiers in Built Environment*, *1*, Article 23. https://doi.org/10.3389/fbuil.2015.00023

Subedi, M., & Acharya, I. P. (2022). Liquefaction hazard assessment and ground failure probability analysis in the kathmandu valley of nepal. *Geoenvironmental Disasters*, *9*(1), Article 1. https://doi.org/10.1186/s40677-021-00203-0